Journal of Thermal Science and Technology

Vol. 2, No. 1, 2007

Flow Field of Turbulent Premixed Combustion in a Cyclone-Jet Combustor*

Kazuhiro YAMAMOTO** Satoshi INOUE** Hiroshi YAMASHITA**
Daisuke SHIMOKURI***, and Satoru ISHIZUKA***
** Department of Mechanical Science and Engineering
Nagoya University, Furo-cho, Chikusa-ku, Nagoya, Aichi 464-8603, JAPAN
E-mail: kazuhiro@mech.nagoya-u.ac.jp
*** Department of Mechanical Engineering
Hiroshima University, 1-4-1 Kagamiyama, Higashihiroshima, Hiroshima 739-8527, JAPAN

Abstract

The flow field in highly turbulent premixed combustion has been examined, using a cyclone-jet combustor. The shear-strain rate is obtained by PIV system. Results show that, in combustion field, mean axial velocity does not decay along center axis and RMS fluctuation velocity is much lower, compared with those in cold flow. The reaction zone detected by an ion probe well corresponds to region of large shear-strain rate. In combustion, turbulence is small around reaction zone to have the undiminished jet velocity, which leads to an increase in length of potential core, although the flame generated turbulence is observed through flow expansion.

Key words: Flame, Premixed Combustion, Turbulence, PIV, Jet

1. Introduction

For modeling turbulent combustion, numerous studies have been made [(1)-(5)]. In these studies, several different regimes have been proposed to classify the premixed flame structure with a phase diagram. Recently, by the drastic improvement of laser diagnostics, it has been possible to obtain two-dimensional flame structure in detail. For example, Buschmann et al.[(6)] have examined the thermal structure by LIF/Rayleigh measurements. Cheng et al.[(7)] have obtained the flow and scalar fields using PIV/OH-LIF to investigate the turbulence and scalar transport.

Nowadays, the existence of distributed reaction zone regime is questionable, and a new phase diagram has been proposed to modify the flamelet region with thin-reaction-zones regime [(8)-(10)]. It has been experimentally confirmed that the reaction zone is kept thin while the preheat zone is thickened, which is in accordance with consideration that small eddies can penetrate into the preheat zone but not into the reaction zone. In our experiments, we use a cyclone-jet combustor to investigate the premixed flame structure in a highly turbulent flow [(11),(12)]. The estimated reaction zone thickness is almost constant even for Ka > 1, and the persistence of laminar flamelet structure is observed. It could be concluded that the reaction region remains undisturbed with thin reaction zone under highly turbulent conditions.

For more discussion on the flame structure affected by small-scale turbulence, it is important to evaluate the flow characteristics such as mean velocity, RMS of velocity fluctuation, and turbulence scale in combustion. In this study, we investigate the flow field in highly turbulent combustion, using the cyclone-jet combustor. Flow measurements are conducted using a Particle Image Velocimetry (PIV) technique for visualizing the two-dimensional velocity field [(13)-(16)], which can substantially reduce test run time and

*Received 18 Dec., 2006 (No. 06-0282)
[DOI: 10.1299/jtst.2.90]

positioning error compared to point-based laser techniques. Based on velocity fields in cold jet and combustion, we discuss an effect of the flame and the turbulent transport in combustion.

2. Experimental

Figure 1 shows a cyclone-jet combustor used in this study. It is possible to investigate turbulent flames over a wide range of turbulence intensities [11),(12),(17,)(18)]. It consists of a combustion chamber with a main jet nozzle and four cyclone nozzles for pilot flames. The diameter of the main jet nozzle, d, is 12.7 mm. The cyclone combustor is of 27 mm i.d. and 23 mm height, with four cyclone nozzles of 2.4 mm i.d. Its exit diameter is 21 mm. The fuel is propane. In the experiment, we vary the mean exit velocity, U_m, and the equivalence ratio, ϕ_m, of the main jet, with a fixed condition of pilot flames for U_p = 10 m/s and ϕ_p = 0.7 to minimize effects of pilot flames. The velocity is from 5 to 30 m/s, and the equivalence ratios are 0.75 and 0.90. The Reynolds number using the diameter of the main jet nozzle and mean exit velocity is from 4100 to 24600 for U_m = 5 to 30 m/s. The mass flow ratios of pilot flow to the main jet are 28.6 % for 5 m/s to 4.8 % for 30 m/s. In our preliminary experiments, we have confirmed that LDV and PIV data show good agreement [19]. Some errors may appear when more seeding particles pass through the laser sheet in large swirl flow. Then, it is expected that the swirl flow is weak. The direct photographs of flames in the cyclone-jet combustor are shown in Fig. 2. As seen in this figure, the flame length is larger as the exit velocity is increased. As the equivalence ratio approaches unity (stoichiometry), the flame becomes shortened. These characteristics are similar to that of a so-called Bunsen flame.

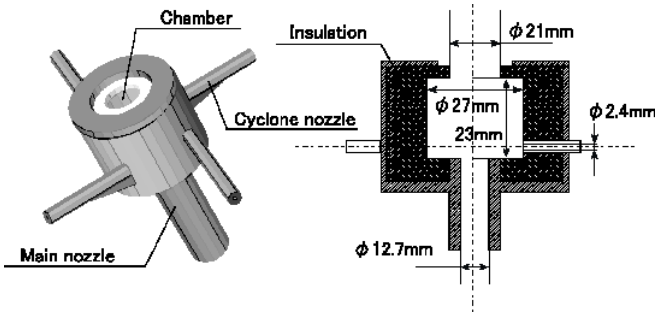

Fig. 1 Cyclone-jet combustor

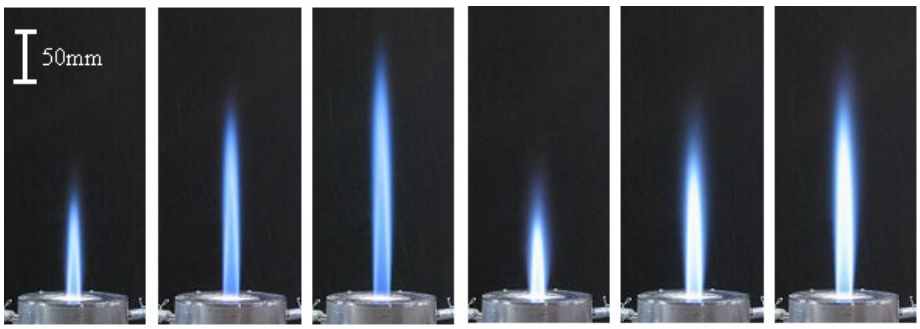

Fig. 2 Photographs of flame in a cyclone-jet combustor; (a) U_m = 10 m/s, ϕ_m = 0.75, (b) U_m = 20 m/s, ϕ_m = 0.75, (c) U_m = 30 m/s, ϕ_m = 0.75, (d) U_m = 10 m/s, ϕ_m = 0.90, (e) U_m = 20 m/s, ϕ_m = 0.90, and (f) U_m = 30 m/s, ϕ_m = 0.90

The experimental conditions have been evaluated in our previous experiments [12]. The turbulent Reynolds number, Re_T, varies from 96 at U_m = 5 m/s to 448 at U_m = 30 m/s, for ϕ_m = 0.75 and 0.9 in this experiment. Based on the phase diagram in Fig. 3, the condition of U_m < 15 m/s for ϕ_m = 0.75 or U_m < 20 m/s for ϕ_m = 0.90 belongs to the flamelet regime, and that of U_m > 20 m/s for ϕ_m = 0.75 or U_m = 30 m/s for ϕ_m = 0.90 belongs to the thin reaction zones regime. In this figure, u' is the RMS velocity, S_L is the laminar burning velocity, l is the integral length, and δ_L is flame thickness. As for the coordinate, Z represents the axial distance from the burner exit, and r is the radial distance from the center axis. Temperature is measured with a silica coated Pt/Pt-13% Rh thermocouple with wire diameter of 50 μm.

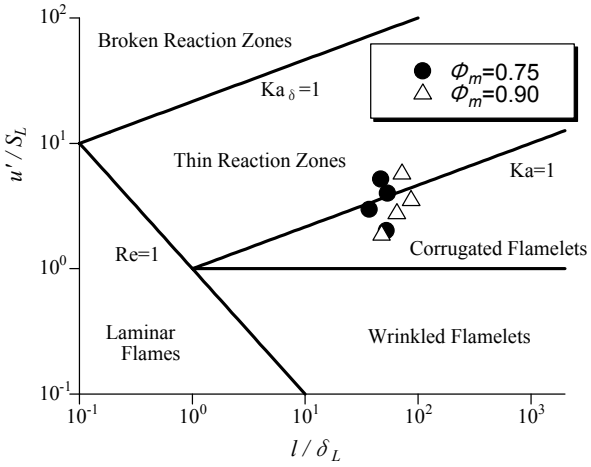

Fig. 3 Combustion diagram for turbulent premixed flames

We use an electrostatic probe to detect the reaction zone, where the ion-electron formation and recombination reactions occur [20],[21]. The ion probe consists of a platinum wire sensor of 0.1 mm in diameter and 0.5 mm long. The sensor projected from a fine quartz tube over which a water-cooled tube is fitted to prevent the quartz tube from the thermal dielectric breakdown. The potential drop across the load resistance is amplified to obtain ion currents, which are stored in the computer. The sampling frequency is 50 kHz. Here, we obtain the reaction variable, a, whose value is unity inside the reaction zone, and zero outside the reaction zone [11],[12]. Then, we determine the probability of reaction zone existing, p, which is the time-averaged value of reaction variable at the specified location.

$$p(Z,r)=\frac{1}{T}\int_0^T a(Z,r,t)dt=\frac{1}{T}\sum_i \Delta t_i \qquad (1)$$

where T is the period of time averaging, and Δt_i is the detected time of reaction region. It should be noted that this reaction variable is different from the so-called progress variable, c, whose value is zero in unburned gas and unity in burned gas [22].

The particle image velocimetry (PIV) system consists of a Nd:YAG laser (TSI Y120-15) and CCD camera (TSI PIVCAM13-8). The 532-nm frequency-doubled beam is used to produce laser sheet of 500 μm thickness through the center of the burner. The time between two PIV pulses are remained constant at 20 μs, and two consecutive raw PIV images are collected on the 1024×1280 pixel array of the CCD camera. The spatial resolution is about 100 μm. This resolution should be compared to the scales of turbulence, for example, the Taylor microscale, $\lambda \approx u'(\nu/\varepsilon)^{1/2}$ (where ν is the kinematic viscosity and ε is the kinetic energy dissipation), and Kolmogorov scale, $\eta = (\nu^3/\varepsilon)^{1/4}$. For the highest turbulent case at U_m = 30 m/s in this experiment, $\lambda \approx$ 1 mm and η = 40 μm, indicating that the Taylor microscale is resolved, but the Kolmogorov scale is far from being resolved for

the velocity measurements.

The velocity component is evaluated using the standard cross-correlation method, with interrogation window of 16^2 pixels overlapped by 50 %, providing a matrix of 127×159 displacement vectors. The axial velocity is u, and the radial velocity is v in this study. The effective vector resolution is about 0.5 mm^3. MgO of 1.8 μm mean diameter is used for particle scattering. The background flame emission is suppressed with the interference filter centered at 532nm with a 10-nm bandpass. To confirm the validity of PIV data, LDV system is also coupled. The experimental uncertainty of PIV measurements in flames has been discussed [14),(23)]. The resulting errors for a strain-rate calculation would be about 100 1/s. These are relatively small in the present study, considering strain rates around the reaction zone ranged from 5000 to 26000 1/s in Figs. 12 to 14.

3. Results

3.1 Flow Field

First, to reveal the flow characteristics in the cyclone-jet combustor, the flow field is examined. Figure 4 shows the example of instantaneous velocity field by PIV in cold flow and combustion (ϕ_m = 0.75). The mean exit velocity, U_m, is 30 m/s. In cold flow (Fig. 4(a)), the large velocity fluctuation is observed at the exit of the burner. The vortices are formed, shown by the arrows. This is caused by shear flow between the center jet and the outer stationary air. It is noted that, by averaging the instantaneous flow field, the velocity profile is similar to the so-called jet flow, which is discussed later. Figure 4(b) shows the flow field in combustion. Compared with the profile in cold flow, the velocity around the center is large even in downstream.

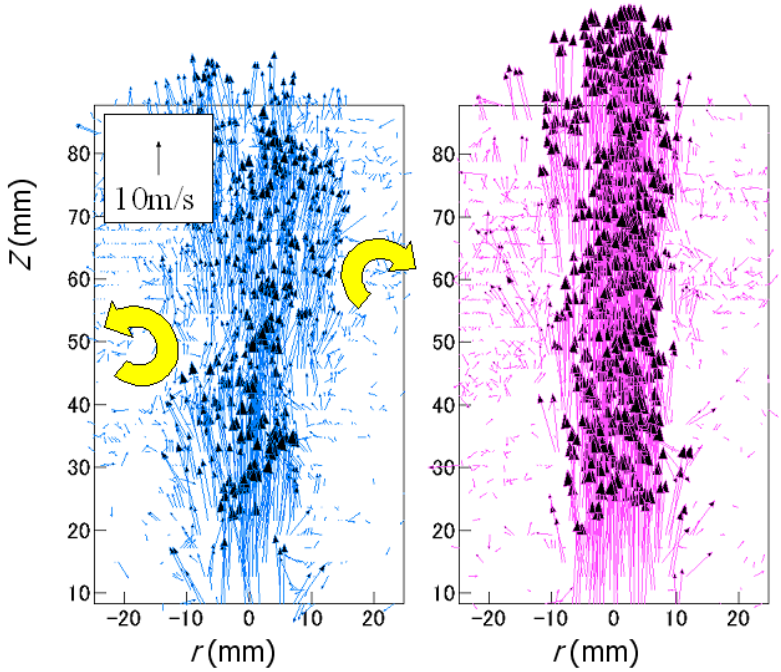

Fig. 4 Velocity field at U_m = 30 m/s; (a) cold flow, (b) combustion (ϕ_m = 0.75)

Figure 5 shows the instantaneous velocity field in combustion. The exit velocities, U_m, are 30 m/s, and the equivalence ratio, ϕ_m, is 0.75 and 0.90. Although it is expected that the flame temperature is higher for ϕ_m = 0.90, the clear difference is not observed between two images.

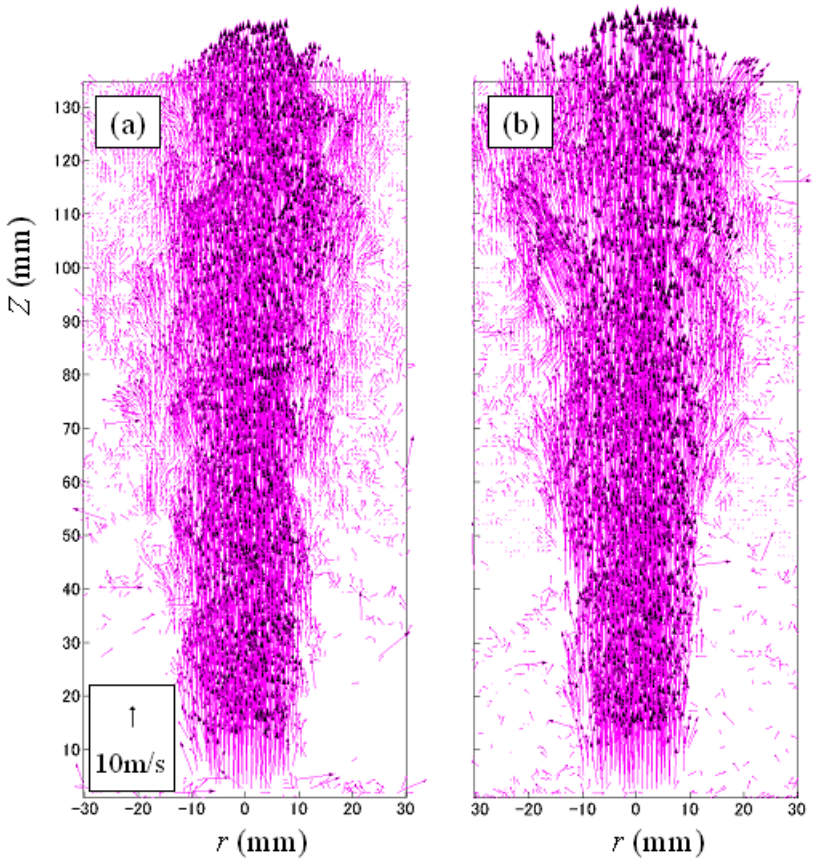

Fig. 5 Velocity field in combustion at U_m = 30 m/s; (a) ϕ_m = 0.75, (b) ϕ_m = 0.90

3.2 Mean and RMS velocity profiles

Next, we examine the flow field in combustion quantitatively based on the turbulence properties using 2000 images, which are compared with those in cold flow. Figure 6 shows mean velocity and RMS of velocity fluctuation along the center axis for U_m = 30 m/s and ϕ_m = 0.75. To discuss further, the axial profiles of time-averaged temperature, T, and ion current, I, are also shown. It is found that these profiles are largely changed with combustion. That is, in cold flow, the mean velocity immediately starts to decrease around Z = 20 mm, with larger RMS of velocity fluctuation. On the other hand, the velocity in combustion is almost constant even relatively downstream. In temperature profile, at Z > 30 mm, the temperature starts to increase monotonically. At Z < 60 mm, since the ion current is still zero, this area is the preheat region. After that, the ion current becomes large. Then, the reaction region is fluctuating around Z = 60 ~ 200 mm.

In this study, we use an ion probe to detect the reaction zone. Although this is a point-measurement, we can obtain the information on whether the reaction occurs or not at the specified time and space. Here, we determine the probability of reaction zone existing, p. An example of signal waveform of ion current is shown in Fig. 7 for U_m = 15 m/s at r = 9 mm and Z = 20 mm [12]. We use simple threshold procedure. As seen in this figure, the ion current signals are binarized with reaction variable, a, whose value is unity or zero. If the ion current is higher than the threshold, it is considered that the probe is located in the reaction region and the reaction variable is set to be unity, whereas if the ion current is lower than the threshold, a is zero. According to Suzuki et al.[21], ion current signal depends on the angle between the flame and the ion probe, and takes its maximum when the flame front is parallel to the sensor. We adopt the half value of maximum ion current as threshold,

I_{th}. Based on Eq. (1), we determine the reaction zone existing by 65000 sampling data. Although the choice of threshold could be sensitive to the detection of reaction region, the validity of our procedure has been already confirmed [12].

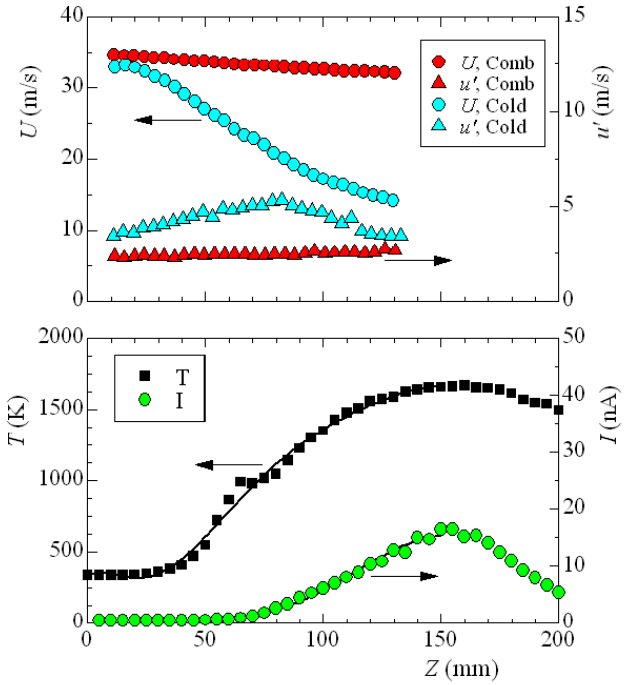

Fig. 6 Axial distributions of mean and RMS longitudinal velocities in cold flow and combustion. For comparison, mean temperature and ion current in combustion are also shown.

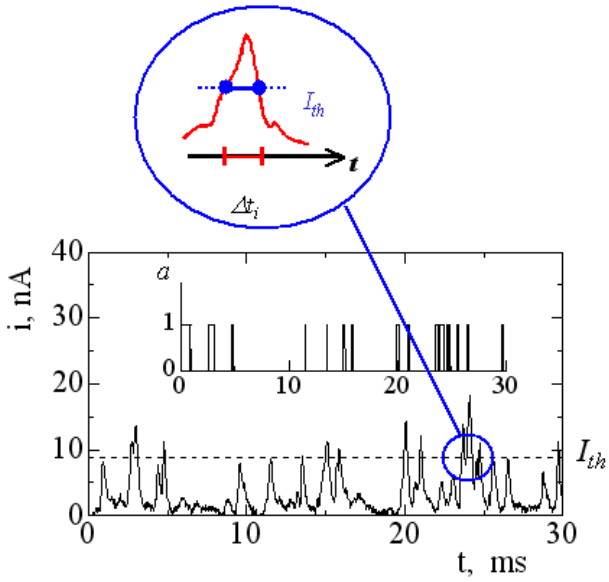

Fig. 7 Signal waveform of ion current and reaction variable; U_m = 15 m/s, r = 9 mm, Z = 20 mm, ϕ_m = 0.75 [12]

Figures 8 and 9 show the radial profiles of mean and RMS of axial velocities in combustion. The exit velocity, U_m, is 30 m/s and the equivalence ratio, ϕ_m, is 0.75. For comparison, those in cold flow are shown. The axial heights, Z, are 10, 30, 50, and 100 mm.

Hatching in these figures shows the reaction region specified by the reaction zone existing. It is found that the reaction region is wider in the downstream, corresponding the larger flame motion, although the radial thickness is not changed up to 50 mm, supported by the fact that the flame diameter is almost constant in Fig. 2.

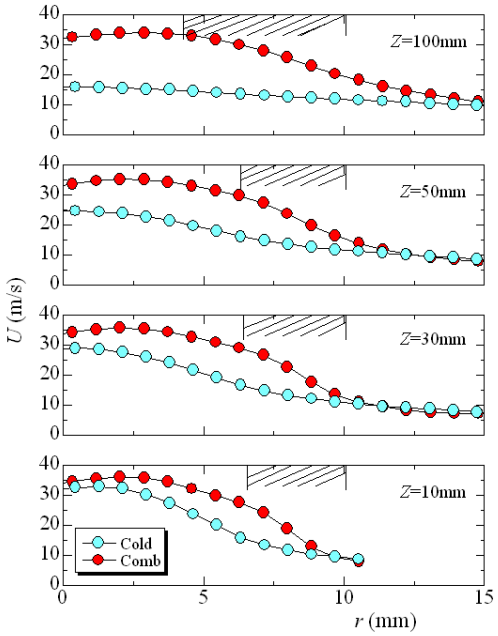

Fig. 8 Radial distributions of mean longitudinal velocity in cold flow and combustion; U_m = 30 m/s, ϕ_m = 0.75

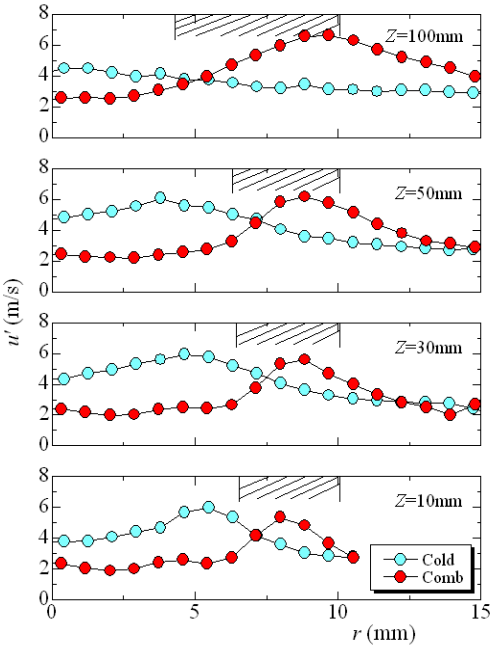

Fig. 9 Radial distributions of RMS longitudinal velocity in cold flow and combustion; U_m = 30 m/s, ϕ_m = 0.75

As seen in Fig. 8, at r > 10 mm, which is around the rim of the combustor, both velocities are almost the same. However, except for this area, the velocity in combustion is always larger. This could be a gas expansion in combustion. On the other hand, the RMS velocity in the center region of unburned gas in Fig. 9 is much lower in combustion. The

turbulence is increased around the reaction region, corresponding to the well-known flame generated turbulence [24].

4. Discussion

Here, we discuss the flow field in combustion to consider the interaction between flame and flow. As seen in Fig. 6, the large difference is observed between axial velocity profiles in cold flow and in combustion. Chen et al.[25] have investigated flow field in a Bunsen flame with low level of turbulence. It has been reported that around the center axis, the mean velocity in combustion is almost constant and the turbulent kinetic energy is relatively low. On the other hand, the velocity decays much faster in the cold jet and turbulence energy rises sharply at the end of the potential core. These are very similar to our results. To discuss further, we examine the flow field by PIV measurement.

Han et al. have measured velocity field by PIV, coupled with CH-PLIF (Han and Mungal[23]). They have found that the CH layer is matched with the region of large shear-strain rate, S, defined by

$$S = \frac{1}{2}\left(\frac{\partial v}{\partial z} + \frac{\partial u}{\partial r}\right) \qquad (2)$$

Since CH exists in the reaction zone, S could be a good maker of the reaction zone. Mueller and Driscoll[26] have pointed out that the clear correlation exists between the shear-strain rate and the reaction zone, especially in premixed flames. Hence, we obtain this shear-strain rate based on PIV data. Figure 10 shows the radial profile of the mean shear-strain rate at Z = 20 mm. For comparison, the probability of reaction zone existing is also shown. The burner rim is located at r = 10.5 mm. We confirm that the region of large shear-strain rate well corresponds to the reaction zone. Then, we examine the profiles of velocity and shear-strain rate.

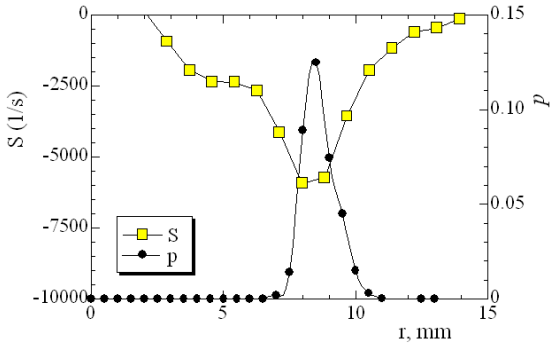

Fig. 10 Distributions of shear-strain rate and probability of reaction zone existing; Z = 20 mm, U_m = 30 m/s, ϕ_m=0.75

Figure 11 shows the instantaneous shear-strain rate in combustion. The exit velocity is 30 m/s, and the equivalence ratios are 0.75 and 0.90. The velocity vector at different axial position is also shown. The shear-strain rate is large around r = 8 to 9 mm. For ϕ_m = 0.9, the flame temperature is expectedly high, and the shear-strain rate is slightly larger. It seems that the area of undiminished jet velocity is surrounded by the reaction zone. To discuss the local flow structure and turbulence, the mean shear-strain rate is plotted with RMS longitudinal velocity in Fig. 12. It is interesting to note that both shear-strain rate and turbulence described by RMS longitudinal velocity are large in the reaction region, but the turbulence decays very rapidly in the burned gas region (r > 10 mm). Since the temperature becomes high in combustion, there are two major effects; one is the heat expansion, and the

other is the increased viscosity. As seen in combustion flow seen in Figs. 6 and 9, the velocity fluctuation of the unburned gas region is largely suppressed, except for that the so-called flame generated turbulence caused by the heat expansion. In that case, it is expected that turbulent transport is much reduced in combustion.

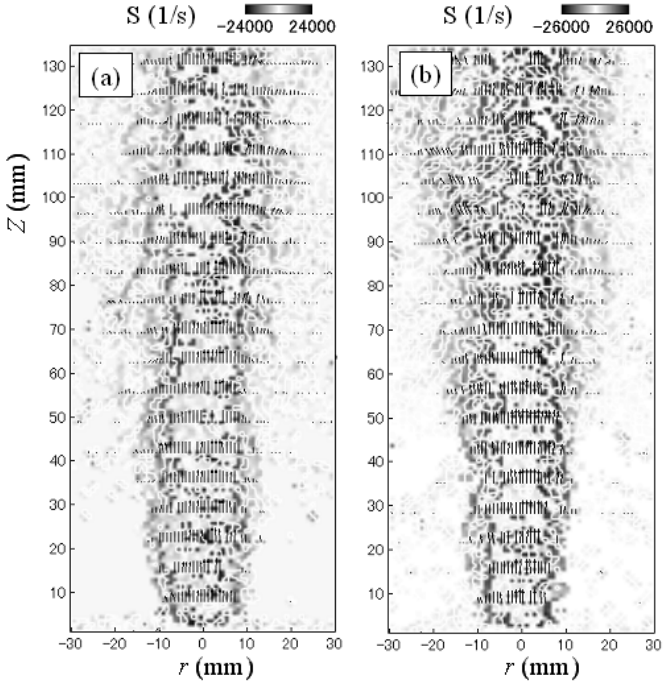

Fig. 11 Profiles of shear-strain rate with velocity vector in combustion, U_m = 30 m/s; (a) ϕ_m = 0.75, (b) ϕ_m = 0.90

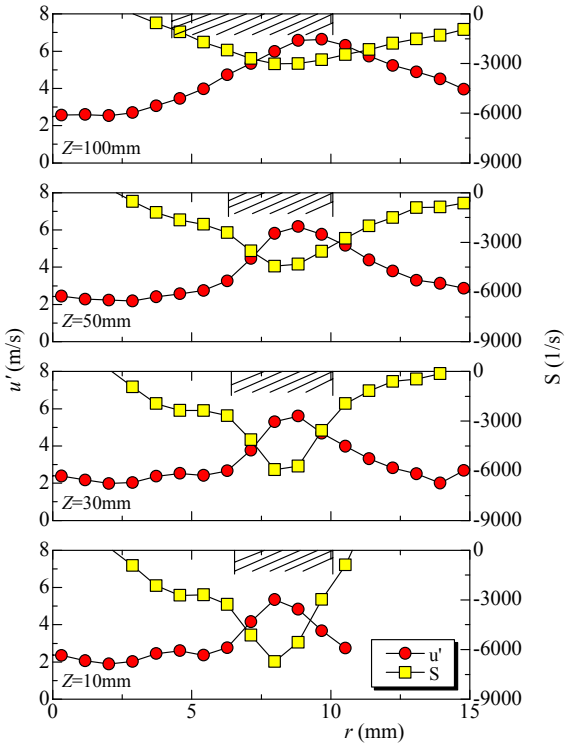

Fig. 12 Distributions of RMS longitudinal velocity and shear-strain rate; U_m = 30 m/s, ϕ_m=0.75

Here, to see the turbulent transport in the longitudinal and lateral direction, the degree of isotropy of the flow is evaluated. In an isotropic flow, the ratio, u'/v', must be strictly unity, where v' is RMS of the lateral velocity. For a straight test chamber, u'/v' is in the range between 1.1 and 1.4 [27]. In the case of an axisymmetric cold jet, the value of u'/v' is 1.0 [28] to 1.44 [29]. Results along the center axis are shown in Fig. 13. The exit velocity, U_m, is 30 m/s and the equivalence ratio, ϕ_m, is 0.75. For comparison, the region where $1.1 < u'/v' < 1.4$ is shown by two solid lines. Both values in cold flow and combustion are compared.

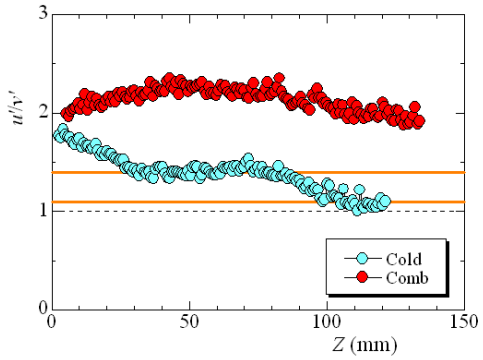

Fig. 13 Ratio between longitudinal and lateral turbulence level in cold flow and combustion; U_m = 30 m/s, ϕ_m = 0.75

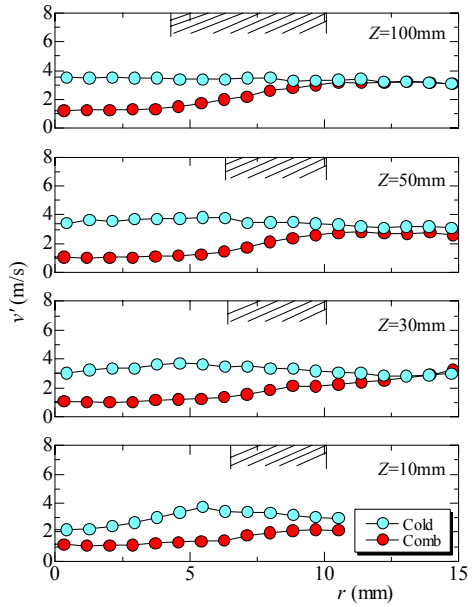

Fig. 14 Radial distributions of RMS lateral velocity in cold flow and combustion; U_m = 30 m/s, ϕ_m = 0.75

In cold flow, u'/v' is higher than 1.4 at $Z < 30$ mm. Since the mean velocity in Fig. 6 does not decay much, this region corresponds to the potential core, and the strong anisotropy is observed. At $Z > 30$ mm, u'/v' is within the level of the straight test chamber. On the other hand, u'/v' in combustion is always higher than 1.4. Figure 14 shows the radial distributions of RMS lateral velocity in cold flow and combustion for U_m = 30 m/s, ϕ_m = 0.75. By comparing the level of u' and v', the lateral turbulence is much decreased in combustion. Hence, the difference of velocity profile between cold flow and combustion is

caused by the reduced turbulent transport. In combustion field, due to increase in temperature, the viscosity is increased and the density is decreased, resulting in the large kinematic viscosity. Then, the turbulence is small around the reaction zone, which leads to an increase in length of potential core. Although the flame generated turbulence is observed through flow expansion, the turbulent transport in the unburned jet is suppressed to sustain the large axial velocity around the center axis, which is well observed in Fig. 11. These findings are supported with the recent experimental results that the reaction zone thickness is not influenced by turbulence in the thin reaction zones regime (De Goey et al.[10]).

5. Conclusions

The flow field in highly turbulent combustion has been examined by a Particle Image Velocimetry (PIV) system. The turbulent flames are stabilized in a cyclone-jet combustor over a wide range of turbulence intensities, for both the flamelet regime and the thin reaction zones regime on combustion diagram. The shear-strain rate is obtained based on two-dimensional velocity measurement. Results show that, the mean axial velocity does not decay along the center axis and RMS fluctuation velocity is much lower, compared with those in cold flow. The reaction zone detected by an ion probe well corresponds to the region of large shear-strain rate. In combustion, the turbulence is small around the reaction zone to have the undiminished jet velocity, which leads to an increase in length of potential core and also in length of anisotropy structure of turbulence, although the flame generated turbulence is observed through flow expansion.

References

(1) Damköhler, G., Z. Elektrochem. Angew. Phys. Chem, Vol.46, (1940), pp.601-626.
(2) Yoshida, A., and Tsuji, H., Measurements of fluctuating temperature and velocity in a turbulent premixed flame. Proc. Comb. Inst., Vol.17, (1978), pp.945-956.
(3) Bray, KNC., and Moss, JB., A unified statistical model of the premixed turbulent flame. Acta Astronautica, Vol.4, (1977), pp.291-319.
(4) Borghi, R., in Recent Advances in Aeronautics Science. Plenum, New York, (1985), pp.117-134.
(5) Peters, N., The turbulent burning velocity for large-scale and small-scale turbulence. J. Fluid Mech., Vol.384, (1999), pp.107-132.
(6) Buschmann, A., Dinkelacker, F., Schafer, T., and Wolfrum, J., Measurement of the instantaneous detailed flame structure in turbulent premixed combustion. Proc. Comb. Inst., Vol.26, (1996), pp.437-445.
(7) Cheng, YC., and Bilger, RW., Turbulence and scalar transport in premixed Bunsen flames of lean hydrogen/air mixtures. Proc. Comb. Inst., Vol.28, (2000), pp.521-528.
(8) Mansour, MS., Peters, N., and Chen, YC., Investigation of scalar mixing in the thin reaction zones regime using a simultaneous CH-LIF/Rayleigh laser technique. Proc. Comb. Inst., Vol.27, (1998), pp.767-773.
(9) Sankaran, V., and Menon, S., Structure of premixed turbulent flames in the thin-reaction-zones regime. Proc. Comb. Inst., Vol.28, (2000), pp.203-209.
(10) De Goey, LPH., Plessing, T., Hermanns, RTE., and Peters, N., Analysis of the flame thickness of turbulent flamelets in the thin reaction zones regime. Proc. Comb. Inst., Vol.30, (2005), pp.859-866.
(11) Yamamoto, K., Nishizawa, Y., and Onuma, Y., Reaction Zone Thickness of Turbulent Premixed Flame. J. The Korean Society of Combustion, Vol.6, (2001), pp.36-42.
(12) Yamamoto, K., Nishizawa, Y., and Onuma, Y., Persistence of laminar flamelet structure under highly turbulent combustion. JSME Int. J, Series B, Vol.47, (2003), pp.408-415.
(13) Frank, JH., Lyons, KM., and Long, MB., Simultaneous scalar/velocity field measurements in turbulent gas-phase flows. Combust. Flame, Vol.107, (1996), pp.1-12.

(14) Rehm, JE., and Clemens, NT., The relationship between vorticity/strain and reaction zone structure in turbulent non-premixed jet flames. Proc. Comb. Inst., Vol.27, (1998), pp.1113-1120.
(15) Kalt, PAM., Chen, YC., and Bilger, RW., Experimental investigation of turbulent scalar flux in premixed stagnation-type flame. Comb. Flame, Vol.129, (2002), pp.401-415.
(16) Hirasawa, T., Sung, CJ., Joshi, A., Yang, Z., Wang, H., and Law, CK., Determination of laminar flame speeds using digital particle image velocimetry: binary fuel blends of ethylene, n-butane, and toluene. Proc. Comb. Inst., Vol.29, (2002), pp.1427-1434.
(17) Yamamoto, K., Achiha, T., and Onuma, Y., A study on highly turbulent premixed flames in a cyclone-jet combustor (1st Report, Visualization of flame structure with tomographic images). Trans. Japan Society of Mechanical Engineers, Series B, Vol.65, (1999), pp.3185-3190.
(18) Yamamoto, K., Nishizawa, Y., and Onuma, Y., A study on highly turbulent premixed flames in a cyclone-jet combustor (3rd Report, Measurement of turbulence scale in combustion field by slot-correlation method). Trans. Japan Society of Mechanical Engineers, Series B, Vol.68, (2002), pp.603-609.
(19) Yamamoto, K., Inoue, S., Yamashita, H., Shimokuri, D., Ishizuka, S., and Onuma, Y., PIV Measurement and Turbulence Scale in Turbulent Combustion, Trans. Japan Society of Mechanical Engineers, Series B, Vol.71, (2005), pp.2741-2747.
(20) Suzuki, T., Hirano, T., and Tsuji, H., Flame front movements of a turbulent premixed flame. Proc. Comb. Inst., Vol.17, (1978), pp.289-297.
(21) Suzuki, T., Kudo, N., Kawamata, M., and Hirano, T., Simultaneous measurements of gas flow and flame front movement in a turbulent premixed flame zone. Proc. Comb. Inst., Vol.21, (1986), pp.1385-1391.
(22) Bray, KNC., Turbulent Reacting Flows, Topics in Applied Physics 44, Springer-Verlag, London, (1980), pp.115-183.
(23) Han, D., and Mungal, MG., Simultaneous measurements of velocity and CH distributions Part 1: jet flames in co-flow. Combust. Flame, Vol.132, (2003), pp.565-590.
(24) Williams, FA., Combustion Theory. Addison-Wesley Publishing Company, New York, (1985), pp.373-445.
(25) Chen, YC., Peters, N., Schneemann, GA., Wruck, N., Renz, U., and Monsour, MS., The detailed flame structure of highly stretched turbulent premixed methane-air flames. Combust. Flame, Vol.107, (1996), pp.223-244.
(26) Mueller, CJ., and Driscoll, JF., Effects of unsteady stretch on the strength of a freely-propagating flame wrinkled by a vortex. Proc. Comb. Inst., Vol.26, (1996), pp.347-355.
(27) Avallone, G., De Gregorio, F., and Romano, GP., PIV measurements in grid turbulence. 5th Int. Symp. on PIV, (2003), pp.22-24.
(28) Gibson, MM., Spectra of turbulence in a round jet, J. Fluid Mech, Vol.15, (1962), pp.161-173.
(29) Wygnanski, I. and Fiedler, H., Some measurements in the self-preserving jet, J. Fluid Mech., Vol.38, (1969), pp.577-612.